BMC Genomics

METHODOLOGY ARTICLE   **Open Access**

Choice of pre-processing pipeline influences clustering quality of scRNA-seq datasets

Inbal Shainer and Manuel Stemmer*

Abstract

Background: Single-cell RNA sequencing (scRNA-seq) has quickly become one of the most dominant techniques in modern transcriptome assessment. In particular, 10X Genomics' Chromium system, with its high throughput approach, turn key and thorough user guide made this cutting-edge technique accessible to many laboratories using diverse animal models. However, standard pre-processing, including the alignment and cell filtering pipelines might not be ideal for every organism or tissue. Here we applied an alternative strategy, based on the pseudoaligner kallisto, on twenty-two publicly available single cell sequencing datasets from a wide range of tissues of eight organisms and compared the results with the standard 10X Genomics' Cell Ranger pipeline.

Results: In most of the tested samples, kallisto produced higher sequencing read alignment rates and total gene detection rates in comparison to Cell Ranger. Although datasets processed with Cell Ranger had higher cell counts, outside of human and mouse datasets, these additional cells were routinely of low quality, containing low gene detection rates. Thorough downstream analysis of one kallisto processed dataset, obtained from the zebrafish pineal gland, revealed clearer clustering, allowing the identification of an additional photoreceptor cell type that previously went undetected. The finding of the new cluster suggests that the photoreceptive pineal gland is essentially a bi-chromatic tissue containing both green and red cone-like photoreceptors and implies that the alignment and pre-processing pipeline can affect the discovery of biologically-relevant cell types.

Conclusion: While Cell Ranger favors higher cell numbers, using kallisto results in datasets with higher median gene detection per cell. We could demonstrate that cell type identification was not hampered by the lower cell count, but in fact improved as a result of the high gene detection rate and the more stringent filtering. Depending on the acquired dataset, it can be beneficial to favor high quality cells and accept a lower cell count, leading to an improved classification of cell types.

Keywords: Single-cell RNA sequencing, Cell Ranger, Kallisto, Zebrafish, Pineal gland, Alignment, Opsin, 10X genomics

* Correspondence: stemmer@neuro.mpg.de
Max Planck Institute of Neurobiology, Am Klopferspitz 18, 82152 Martinsried, Germany

Background

Single-cell transcriptome sequencing (scRNA-seq) has rapidly become one of the most popular tools for dissecting the transcriptomic states of individual cells in a tissue of interest. It can be applied to virtually any biological sample as long as a reference genome is available. Among the available scRNA-seq techniques, the Chromium (10X Genomics) platform is probably the most widely used at this point. Thanks to its user-friendly design and very well-documented workflow, it has quickly emerged as the top choice for many researchers and clinicians [1–8]. Its droplet-based design and simple workflow make it the ideal technique for surveying hundreds to thousands of cells in a single experiment, without needing prior knowledge of the system [9, 10]. In addition to its hardware, 10X Genomics also provides a whole suite of tools called Cell Ranger for processing sequencing reads (demultiplexing, alignment, filtering, dimensionality reduction and visualization of clusters) (10xgenomics.com). Within this package, STAR [11] is applied to align the millions of short reads, typically produced by Illumina sequencers. This aligner has been shown to work accurately and reliably and is widely used.

Besides STAR and other classic aligners like GSNAP or TopHat2 [11–13], there have been recent advances in the development of so called pseudoaligners. Instead of trying to exactly evaluate the alignment of each base in a given read, pseudoaligners only focus on the potential identity of the target transcript [14]. Among the few existing tools like salmon/alevin, sailfish or kallisto [14–17], kallisto comes with a suite of complementary tools for processing and filtering scRNA-seq reads, making it as simple to use as Cell Ranger. Importantly, the computational resources required for kallisto are marginal in comparison to Cell Ranger/STAR, with an entire scRNA-seq run, can be aligned on a standard laptop within tens of minutes [14, 18] instead of hours for Cell Ranger/STAR. The alignment process is sped up by a magnitude by splitting up the reads into k-mers and matching them using hash tables, while the accuracy is maintained by constructing a transcriptome de Bruijn graph [14, 19]. Kallisto can also align reads coming from bulk RNA-seq, and the introduction of the Barcode-UMI-Set (BUS) format allows processing and comparison of scRNA-seq data originating from various sources [19]. In addition to the alignment of the sequencing reads by either STAR or kallisto, the transcripts have to be associated with their respective cell barcodes and the unique molecular identifiers (UMIs) have to be counted [20]. As a last step, empty droplets are removed from the dataset before one can proceed to downstream processing [21, 22]. All these functions are conveniently included in the Cell Ranger pipeline, but are usually not obvious to the user.

While Cell Ranger is an all-in-one package, the kallisto pipeline consists of three parts. Kallisto [14] aligns the sequencing reads, while bustools [19] associates the reads to the respective cell barcodes, collapses the UMIs, counts the identified transcripts and creates the cell to gene matrix. In the third part we use DropletUtils [23] to rank barcodes according to detected UMI levels and define the inflection point within the resulting knee-plot as a threshold between droplets that are thought to contain cells and empty droplets. The individual packages are all open-source and the process can be inspected in detail [14, 19, 23]. We refer to this entire pipeline as "kallisto".

Although based on the same principles, the underlying approach of kallisto and Cell Ranger differ and so are potentially the resulting datasets. Here we show that alternative alignment strategies can indeed make a difference in the derived biological conclusions, especially when working with organisms other than human or mouse. Using kallisto we found a strong increase in alignment rates (percent of reads aligned to reference transcriptome) and consequent gene detection rates within most of the tested Chromium v2/v3 datasets (zebrafish, killifish, cavefish, drosophila, c. elegans, ciona, mouse, human). Additionally, we show that the choice of reference genome and differences in thresholding empty droplet removal has strong effects on correct filtering and resulting cell counts. Finally we demonstrate, using a dataset obtained from the zebrafish pineal gland [7], that alignment with kallisto and cell filtering with DropletUtils [23] improve clustering quality and reveal new cell types.

Results

To uncover whether the choice of alignment tool affects the downstream results, we analyzed twenty-two published single-cell sequencing datasets from eight different organisms (Table 1). The first difference between the two approaches was the overall higher alignment rates of sequencing reads to the transcriptome for kallisto (on average 7.2% increase) with the only exception of drosophila dataset s1 (Fig. 1a). Furthermore, total gene detection rates were increased in the kallisto samples in comparison to Cell Ranger, with the exception of the *C. elegans* datasets. Most of the identified genes were shared between the two pipelines, but for teleost and mammal samples, kallisto detected considerably more genes than Cell Ranger (Fig. 1b and Additional file 1: Fig. S1). When looking at the median gene count (MGC) and median UMI count (MUC) per cell, we found again increases in the majority of samples processed with kallisto, with one exception: mouse sample mm-neuron-2 k-v2 (Fig. 1c, d). In contrast, cell counts were lower for all samples processed with kallisto, except

Table 1 Datasets and sources

sample ID	organism	common name	tissue	10X version	FACS sorted	source	reference	ensembl reference version
dr-RGC-larva-s1	*D. rerio*	zebrafish	Retinal ganglion cells (RGCs)	2	yes	GSE152842	Koelsch et al., 2020	101
dr-RGC-adult-s17	*D. rerio*	zebrafish	RGCs	2	yes	GSE152842	Koelsch et al., 2020	101
dr-pineal-s1	*D. rerio*	zebrafish	pineal gland	2	no	SRR8315377/ SRR8315378	[7]	101
dr-pineal-s2	*D. rerio*	zebrafish	pineal gland	2	no	SRR8315379/SRR8315380	[7]	101
nf-embryo-s1	*N. furzeri*	killifish	tail blastema	2	no	SRR11886701	[8]	101
nf-embryo-s2	*N. furzeri*	killifish	tail blastema	2	no	SRR11917464	[8]	101
am-hk-cave	*A. mexicanus*	mexican cavefish	head kidney	3	yes	GSE128306/L39134	[6]	100
am-hk-surf	*A. mexicanus*	mexican cavefish	head kidney	3	yes	GSE128306/L39132	[6]	100
dm-brain-s1	*D. melanogaster*	drosophila	brain	2	no	SRR6327103	[2]	100
dm-brain-s2	*D. melanogaster*	drosophila	brain	2	no	SRR6327104	[2]	100
ce-embryo-s1	*C. elegans*	C. elegans	embryo	2	no	SRR8611991	[4]	100
ce-embryo-s2	*C. elegans*	C. elegans	embryo	2	no	SRR8611992	[4]	100
ci-larva-s1	*C. intestinalis*	ciona	larva	2	no	SRR9051005	[1]	100
ci-larva-s2	*C. intestinalis*	ciona	larva	2	no	SRR9051006	[1]	100
hs-pbmc-4 k-v2	*H. sapiens*	human	pbmc	2	no	*	10X Genomics	100
hs-pbmc-8 k-v2	*H. sapiens*	human	pbmc	2	no	*	10X Genomics	100
mm-neuron-2 k-v2	*M. musculus*	mouse	neurons	2	no	*	10X Genomics	100
mm-neuron-9 k-v2	*M. musculus*	mouse	neurons	2	no	*	10X Genomics	100
hs-pbmc-10 k-v3	*H. sapiens*	human	pbmc	3	no	*	10X Genomics	100
hs-pbmc-1 k-v3	*H. sapiens*	human	pbmc	3	no	*	10X Genomics	100
mm-neuron-10 k-v3	*M. musculus*	mouse	neurons	3	no	*	10X Genomics	100
mm-neuron-1 k-v3	*M. musculus*	mouse	neurons	3	no	*	10X Genomics	100

* https://support.10xgenomics.com/single-cell-gene-expression/datasets

for the human samples and mouse sample mm-neuron-1 k-v3 (Fig. 1e).

Both classic aligners as well as pseudoaligners require an annotated reference transcriptome for alignment, which is typically generated from a gene transfer format (GTF) file and corresponding genomic resource. To assess the influence of transcriptome reference choice on alignment results, we ran our zebrafish samples also along a recently improved zebrafish transcriptome annotation (zta) v4.3.2 [24] (Fig. 2). In all the zebrafish datasets, zta v4.3.2 improved the alignment and gene detection rates, while differences in cell counts were minor (Fig. 2). Similar to results seen for the alignment to the Ensembl reference (101), kallisto analyzed datasets had higher MGC and MUC when aligned to zta 4.3.2 in comparison to Cell Ranger. Unlike classic aligners, kallisto also allows alignment to a pure transcriptomic input. This is an advantage for species, where a GTF file and genomic resource are not available. So, in this case we also included a reference extraction from Ensembl's BioMart. Although based on the same Ensembl version, the reference constructed from BioMart contains more transcript annotations. However, it only marginally improved gene detection rates in comparison to the genome annotation (Fig. 2). This analysis shows that the choice of reference can impact total gene detection, MGC, MUC and cell count for both kallisto and Cell Ranger, but regardless the reference choice, Cell Ranger provided higher cell counts, while kallisto resulted in higher total gene detection, MGC and MUC. Additionally, the flexibility of kallisto enables a wider choice of options of alignment references.

Next, we looked at the cellular distribution in relation to their detected genes. Interestingly, all samples processed with Cell Ranger included a population of cells at the lower end of MGCs, at around 300 to 500 genes per cell (Fig. 3 and Additional file 1: Fig. S2 and S3). The only exceptions here were the human samples (Fig. 3f
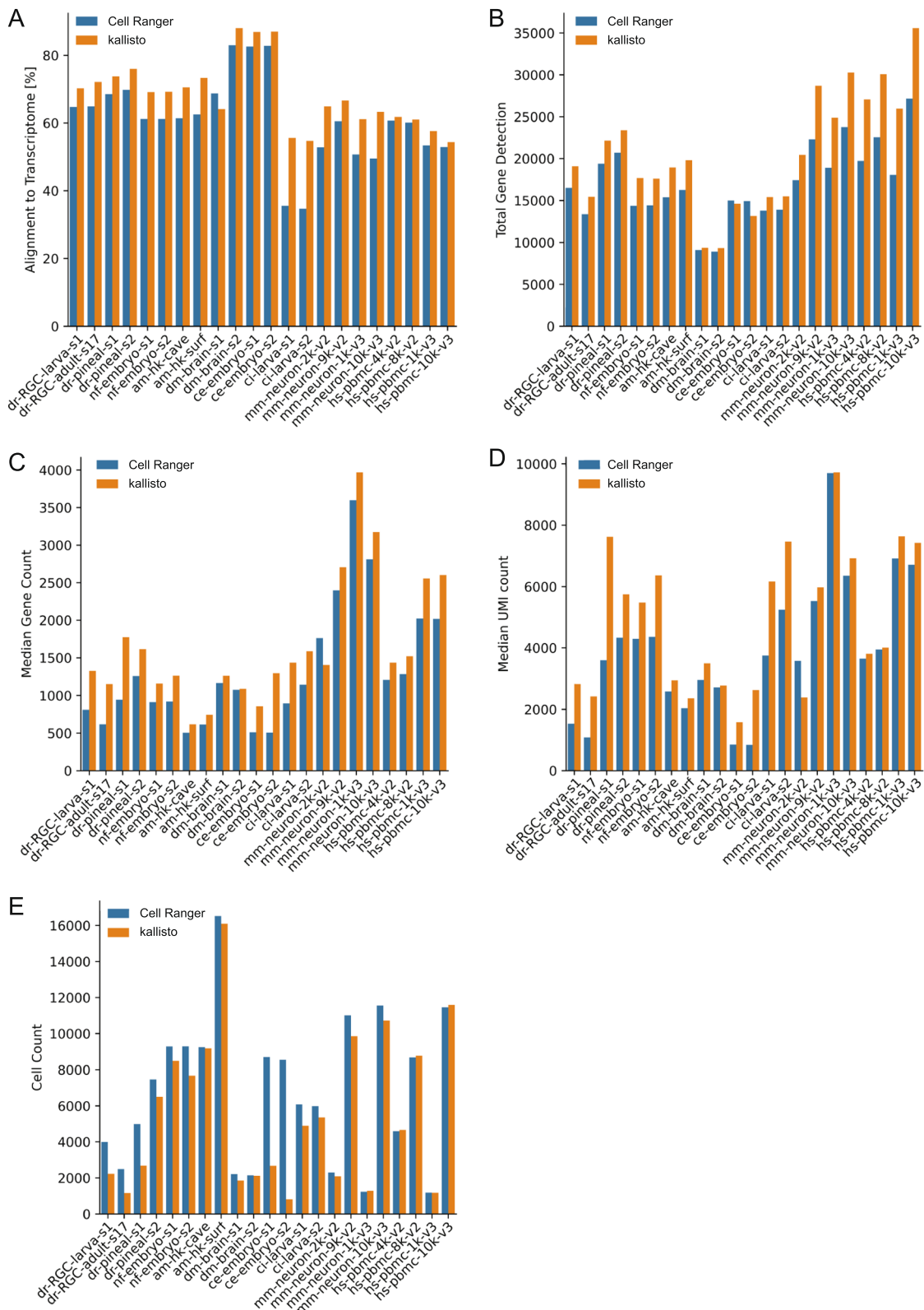
Fig. 1 Alignment results of all datasets (Table 1) run with either Cell Ranger or kallisto against Ensembl reference. **a** Percent alignment rates of reads against the reference transcriptome. **b** Total gene detection. **c** Median gene counts over all cells per dataset. **d** Median UMI counts over all cells per dataset. **e** Total cell counts of each dataset
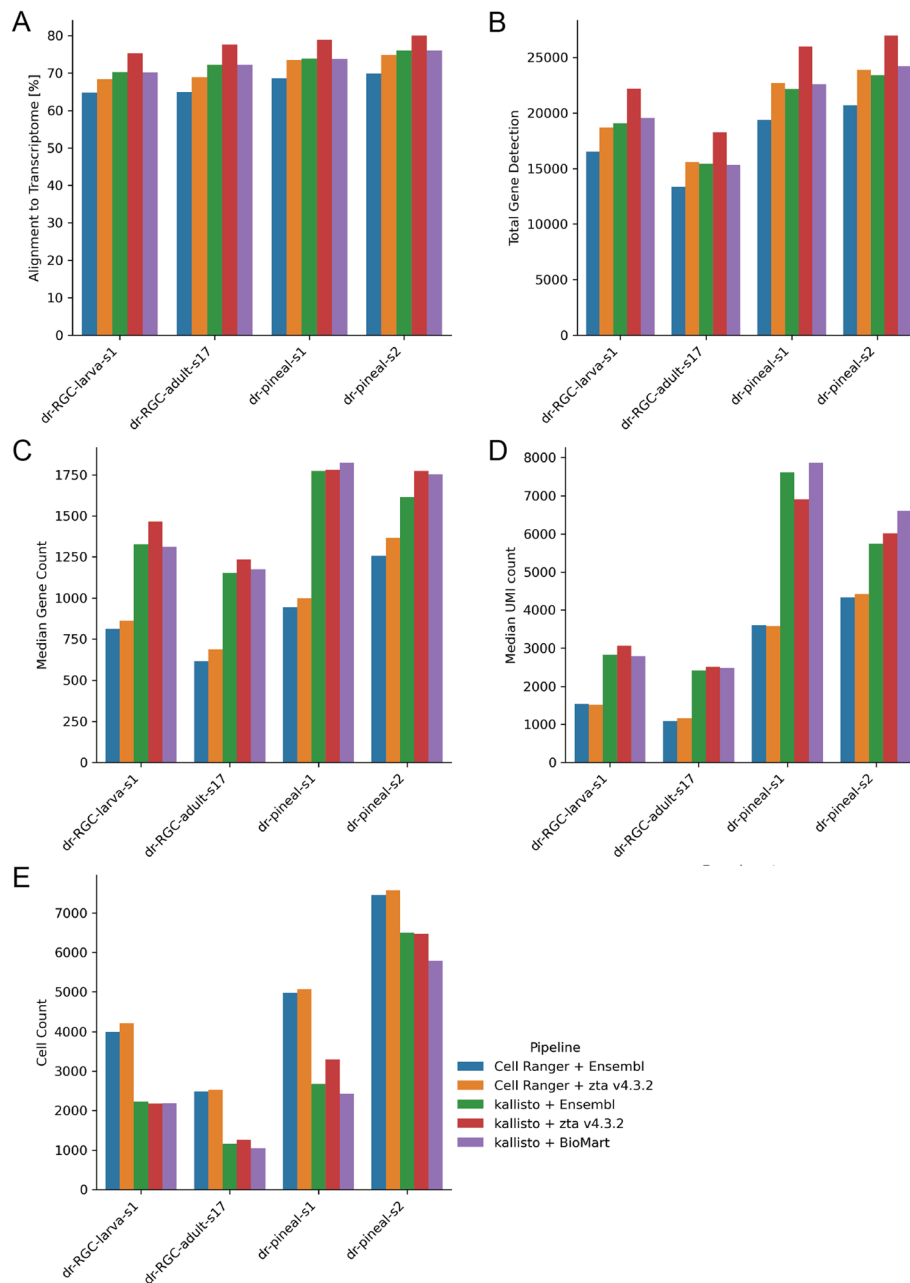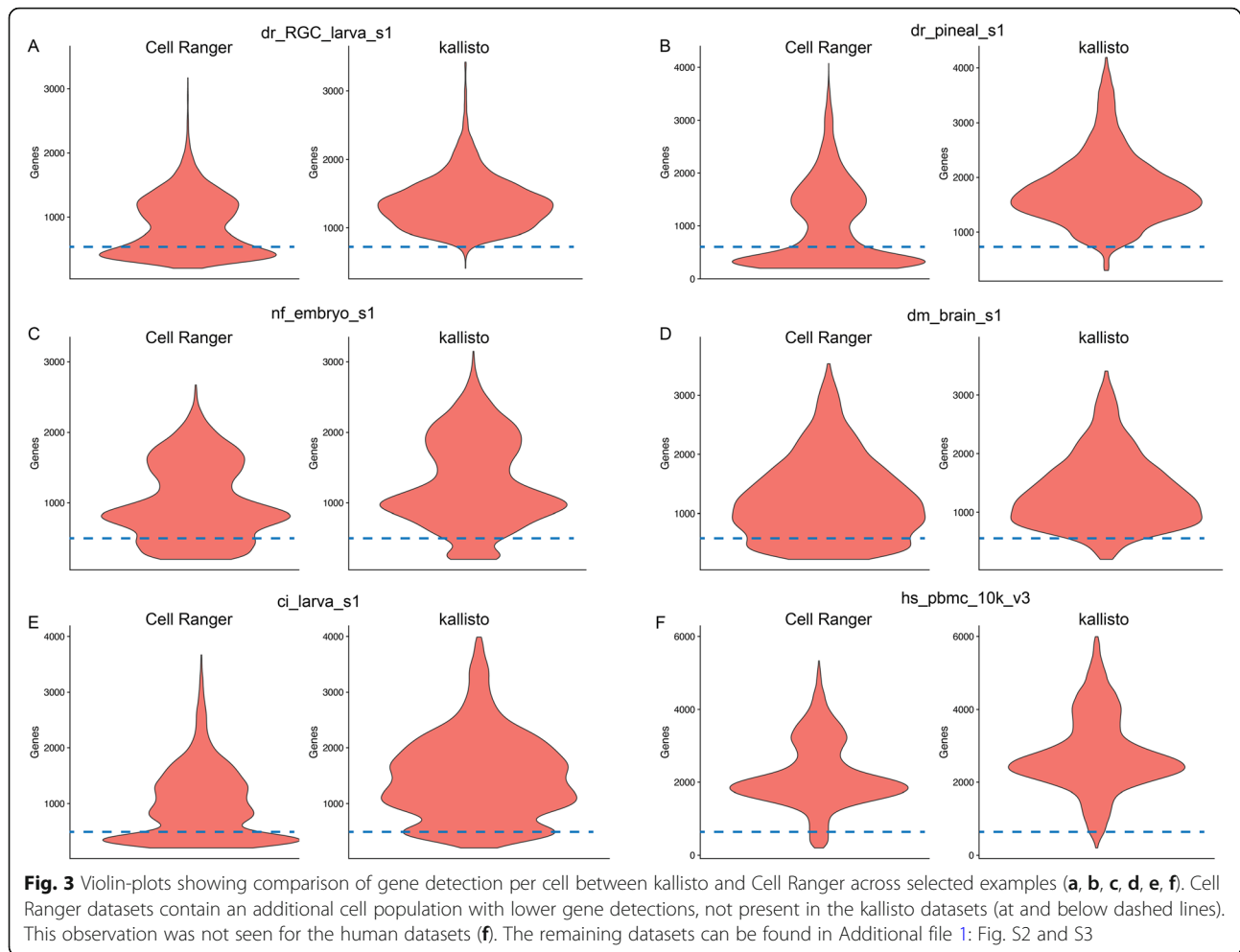
Fig. 2 Impact of reference choice and alignment pipeline on zebrafish scRNA-seq datasets. **a** Percent alignment rates of reads against the reference transcriptome. **b** Total gene detection. **c** Median gene counts over all cells. **d** Median UMI counts over all cells. **e** Total cell counts of each dataset

and Additional file 1: Fig. S2 and S3). This effect was also less pronounced in the mouse datasets (Additional file 1: Fig. S2 and S3). The kallisto pipeline on the other hand excluded most to all of these low MGC cells (Fig. 3 and Additional file 1: Fig. S3).

What is considered a cell in scRNA-seq data is based on finding an appropriate cutoff between what are thought to be empty droplets and droplets containing a cell. Since this is commonly measured only indirectly by

looking at transcript levels beyond a certain threshold in the knee plots, the numbers of cells are heavily dependent on the applied filter [21, 22]. Thus, in a next step we wanted to test, whether the datasets processed with the kallisto pipeline still contain cells with higher MGCs, when the thresholds are set to the same levels as Cell Ranger. Therefore, we did not identify the inflection point automatically using DropletUtils, but forced kallisto to reach similar cell counts as Cell Ranger ('kallisto

Fig. 3 Violin-plots showing comparison of gene detection per cell between kallisto and Cell Ranger across selected examples (**a**, **b**, **c**, **d**, **e**, **f**). Cell Ranger datasets contain an additional cell population with lower gene detections, not present in the kallisto datasets (at and below dashed lines). This observation was not seen for the human datasets (**f**). The remaining datasets can be found in Additional file 1: Fig. S2 and S3

forced'), which resulted in an overlap between the majority of the cell barcodes (Additional file 1: Fig. S4). The very small number of cells, which are either detected by kallisto or Cell Ranger are attributed to the different alignment strategies and corresponding filtering methods.

Kallisto forced still showed overall higher MGCs and MUCs per sample, however less pronounced with one more exception (dm-brain-s1) (Additional file 1: Fig. S5), and the total gene detection slightly increased (Additional file 1: Fig. S6). Interestingly, the population of cells containing low gene count, that was previously only detected within the Cell Ranger data, was now evident (Additional file 1: Fig. S7). Hence, the differences appear to stem from the filtering process taking care of the empty droplet removal.

To test whether the noticeable differences in gene or cell number detection between the two pipelines alter the ability to characterize the cellular composition of the tissue in the downstream analysis, we performed principal component analysis (PCA) and clustering of the zebrafish pineal sample number two (dr-pineal-s2). The

pineal gland dataset was previously studied in high detail by one of the authors [7], and thus represents the ideal basis for comparative downstream analysis. We mainly focus here on the larger dataset, dr-pineal-s2 over dr-pineal-s1, (Fig. 1e), while the complete analysis of dr-pineal-s1 can be found in Additional File 2. We refrained from merging the two datasets, as this was not done in the original publication, making it more comparable to the current analysis.

In the previous analysis of this dataset [7], dr-pineal-s2 was aligned to the zebrafish GRCz10 genome assembly (Ensembl release 90) with Cell Ranger version 2.0.2. A total of 2266 cells were detected [7] and eight cell types, including the pineal gland rod- and cone-like photoreceptors (PhR), five other pineal cell types (retinal pigment epithelium-like, Müller-like glia, neurons, macrophages/microglia and blood cells) as well as habenula neurons [7].

In the current analysis, the dr_pineal_s2 dataset was aligned with Cell Ranger version (v5) to Ensembl release 101, which resulted in more than double of the total number of cells (6769) (Fig. 1e).

The dataset was filtered using similar parameters as in the original publication (see Methods) and the observed cell population with low gene detection in the Cell Ranger object was still present (Additional file 1: S8a). These cells clustered into 13 types (Fig. 4a, b and Additional file 1: Fig. S9a, b and Additional file 3), which included the previously identified clusters as well as two types of habenula cells, erythrocytes, fibroblasts, vascular endothelial cells, leukocytes and epithelial cells (Fig. 4a, b). The additional types of cells, although not identified in the previous study [7], are possibly a result of the higher cell count and improved Cell Ranger version, and expected to reside in the pineal as well as in any other brain tissue.

Analysis of the same dataset using kallisto, resulted in a total number of 5810 cells (Fig. 1e), and the population

of cells with the low gene count was excluded (Additional file 1: Fig. S8b). These cells clustered into 14 types (Fig. 4c, d and Additional file 1: Fig. S9e, f and Additional file 3), which included all the types identified by the Cell Ranger analysis, and an additional cone-like PhR cluster (Fig. 4c, d). For both approaches, the number of cells comprising the cone-like photoreceptors are very similar (121 for Cell Ranger & 119 for kallisto; full list in Additional File 4) and thus the numbers alone are most likely not the reason for the separation of the two cone-like photoreceptors in the kallisto pre-processed data. The two cone-like PhR clusters differed in the opsins they expressed, with one expressing *opn1lw1* and *opn1lw2*, the red opsins (long wavelength sensitive), and the other expressing *parietopsin*, a green opsin. To further explore the discrepancy of the cluster identification
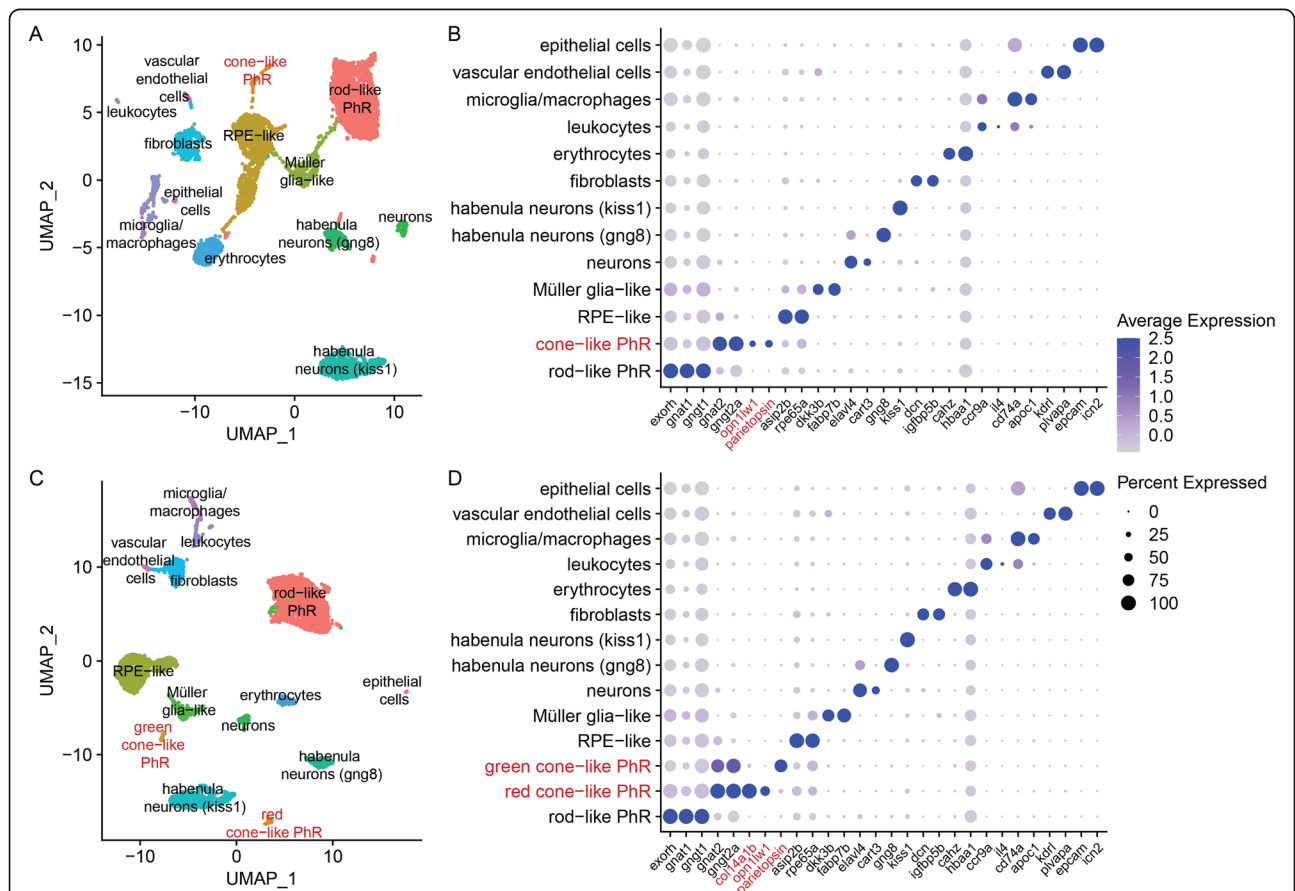
Fig. 4 Downstream analysis of the dr_pineal_s2 dataset. **a** 2D visualization using UMAP of Cell Ranger analyzed clusters. Each point represents a single cell, colored according to cell type. The cells were clustered into 13 distinct types, which were defined according to their unique transcriptomes (Additional file 2). **b** Expression profile of marker genes according to cluster [7] of (**a**). Cone- and rod-like PhRs are defined according to their transducin protein subunits (*gnat1* and *gngt1* in rods vs. *gnat2* and *gngt2a* in cones [25]), as well as their unique opsins (*exorh* in rod-like [26] and *opn1lw1* and *parietopsin* in cone-like). **c** 2D visualization using UMAP of kallisto analyzed clusters. Each point represents a single cell, colored according to cell type. The cells were clustered into 14 distinct types, which were defined according to their unique transcriptomes (Additional file 2). **d** Expression profile of marker genes according to cluster [7] of (**c**). Two different populations of cone-like PhRs are detected. Both express the cone unique transducin protein-subunits, but differ in the expressed opsin (*opn1lw1* in red-cones, and *parietopsin* in green-cones), demonstrating the bi-chromatic photoreception characteristic of the pineal gland. *col14a1b* was only detected in the kallisto dataset and is the strongest DE marker within the red-cone cluster (**c, d**)

between the pipelines, we checked for *parietopsin* expression in the Cell Ranger data (Fig. 4b). Although *parietopsin* was identified within the cone-like PhRs, no distinction between the red and the green cones is made even after more than doubling Seurat's FindClusters resolution parameter (Additional file 1: Fig. S9c, d), which can increase the number of clusters, while preserving dimensional reduction. We refrained from changing any other standard parameter in order to maintain similarity of the pipelines. Analysis of the top differentially-expressed (DE) genes within the cone-like PhRs, revealed that for the kallisto dataset, the gene *col14a1b* (*collagen, type XIV, alpha 1b)* was the most DE gene in the red cone-like PhRs (Fig. 4d and Additional file 3). This gene was not detected at all by the Cell Ranger alignment, and therefor did not exist as a DE gene (Fig. 4b and Additional file 3).

Since the kallisto dataset contains a higher total gene detection rate, we explored whether there is a general trend of counted genes, such as *col14a1b,* that can result in identification of additional clusters. To that end, we compared the UMI counts of all genes identified with kallisto or Cell Ranger and found that for both, there are genes with comparatively higher UMI counts in one pipeline and not the other (Additional File 5). In order to see, whether those genes are detected as cluster-specific markers and thus affecting the downstream analysis, we plotted those genes in heatmaps against the detected clusters (Additional File 1: Figs. S10 &S11). For both pipelines, those genes are spread out over most of the clusters. In the case of kallisto, some genes with high UMI counts, including *col14a1b*, are highly expressed in the cone-like photoreceptor cluster in comparison to the other clusters, suggesting that this led to the identification of the respective cluster. For Cell Ranger, there are also genes with different count ratios, which are differently expressed between clusters, but did not result in new clusters.

A similar trend was also observed for the smaller pineal dataset (dr-pineal-s1). The additional cone-like cluster could also only be identified using the kallisto pipeline. However, Cell Ranger detected two additional clusters, which are not part of the pineal gland (a type of pigment cells representing a "contamination" of the tissue dissection, and hematopoietic cells) (Additional File 2).

To test whether the higher total gene detection rate in the kallisto dataset was the sole cause for identification of the new cluster, or whether the population of cells with the low gene count in the Cell Ranger data hampered its detection, we also performed downstream analysis of the kallisto forced dataset (Additional file 1: Fig. S8c). This data combines the total gene detection rate of kallisto, as well as the population of cells with the low gene count of Cell Ranger. We did not detect the new cluster of the green cone-like PhR in the kallisto forced at the beginning (Additional file 1: Fig. S9e, f). However, increasing the clustering resolution from 0.9 to 1.2 revealed the new cluster (Additional file 1: Fig. S9g, h). With this resolution, the gene *col14a1b* was the most DE gene in the red cone-like PhR for the kallisto forced as well (Additional file 1: Fig. S9h). These findings suggest that not only the additional genes affected the identification of the new cluster, but that the population of cells with low gene count was detrimental to the cell type detection and required a higher resolution to reach the same results.

Discussion

We compared two scRNA-seq read alignment and filtering pipelines; Cell Ranger, the standard tool and part of the 10x Genomics package and the lightweight pseudoaligner, kallisto, on a diverse range of scRNA-seq datasets across the animal phylum. We specifically focused on the latest and most used Chromium chemistries (v2/v3) and compared over a range of different species. Furthermore, we aimed to compare directly with the standard parameters of the Cell Ranger pipeline, as this is the most common way to prepare Chromium scRNA-seq data.

Recent publications comparing STAR and kallisto [27, 28] showed that applying STAR [11] results in better gene detection than kallisto, depending on the applied scRNA-seq technology and reference. On the other hand, a direct comparison between Cell Ranger and kallisto show overall comparable results concerning MGC & MUC and clustering analysis [18]. In another instance, kallisto was reported to detect high cell numbers and cells with low gene content when applied on human and mouse samples [29]. Here we compare kallisto to Cell Ranger, while focusing in more detail on the effects of the pre-processing on the biological relevance of the clustering results. We demonstrate that both differences in the gene detection rate and filtering between the pre-processing pipelines can result in identification of new cell types and improve the overall understanding of tissue composition.

For most of the datasets explored here, kallisto resulted in overall increased alignment rates of the reads to the transcriptome, total gene detection rates, MGC & MUC, in comparison to the standard Cell Ranger pipeline. When looking at cell counts after thresholding out empty droplets, the numbers were higher for most of the samples when run with Cell Ranger. As mentioned before, the number of cells is defined by a threshold drawn between potentially empty and cell containing droplets [21, 22]. This process is quite different between Cell Ranger and kallisto. The cut-off in Cell Ranger was generally much higher, favoring higher cell counts, but

with the potential integration of cells with low gene detection rates (Fig. 3), as seen consistently in all the non-mammalian datasets (Additional file 1: Fig. S2). A similar observation was also made with kallisto [29]. However, this result could simply be derived from different filtering parameters and do resemble our kallisto forced datasets, in which the cutoff in the knee plot was shifted towards higher cell numbers and thus included also cells with lower MGCs. Due to the underlying technology and the lack of ground truth about the exact number of intact cells passing the droplet formation and library preparation, it is difficult to test, whether these are real cells or cells of lower quality [30]. The number of these cells were reduced or not present in the mouse and human samples. One of the reasons could be that the standard parameters of Cell Ranger work better for mouse and human datasets or that these samples were of higher quality to begin with (Fig. 3).

To find out whether the cell population with low gene detection rates impacts the scientific conclusions of underlying biology, we performed clustering analysis of the zebrafish pineal dataset (dr-pineal-s2; Fig. 4). The pineal cellular composition in non-mammalian vertebrates shows similarities to the retina. It is a photoreceptive tissue that regulates circadian rhythms and seasonal changes and therefore contains rod-like and cone-like PhRs [31, 32]. Using kallisto, we were able to further differentiate the cone-like PhRs into two clusters with one distinguished by red opsins (long wavelength sensitive) and the other by green opsins (Fig. 4). This finding suggests that the pineal gland could be a bi-chromatic photoreceptive tissue, containing cones sensitive to different wavelengths. Mutual exclusive expression of *opn1lw1* and *parietopsin* in the pineal cone-like PhRs was recently demonstrated [33], and thus, the additional cluster found with kallisto reflects a true biological finding, previously undetected when using the Cell Ranger platform with the standard parameters. In contrast to the Cell Ranger data, the additional cluster was detected with kallisto forced but only when increasing the clustering resolution (Additional file 1: Fig. S9). Merely due to the increased overall gene detection, it became possible to identify the additional cluster, while it was the altered filtering of the kallisto pipeline that reduced the noisiness in the data and improved cell type detection. Analysis of the additional pineal dataset (dr-pineal-s1), revealed a very similar trend. The additional cone-like photoreceptors could only be found when pre-processing the dataset with kallisto, while two additional clusters, which are not part of the pineal itself, were only detected with Cell Ranger (Additional File 2). These are small clusters that seem to result from cells that were mostly filtered out in the kallisto pre-processing steps. This can also represent a case, where the pre-processing

steps affect the clustering analysis, though by cells filtered out and not by gene detection.

Although all the processing was performed using standard conditions in order to ensure the best comparison between datasets as possible, several steps in the pipelines can be tuned further, which can result in the detection of additional genes and clusters. Thus, we cannot rule out the detection of the green cone-like PhRs with Cell Ranger under non-standard analysis parameters. For instance, one could work with the unfiltered output of Cell Ranger and change the filtering threshold to the knee point instead of the inflection point or use tools like EmptyDrops [21] for this step. Additionally, other parameters in the downstream analysis can be adjusted such as the normalization method, number of variable genes, number of principal components or clustering algorithm. This however might not be applicable for the routine use of scRNA-seq, which is becoming increasingly popular, and also requires an advanced knowledge.

Furthermore, if a certain cell type is expected or if some particular cluster comprises enough cells, one can also isolate those and re-run the analysis to further differentiate the cluster. This requires prior knowledge of the composition of cell types and the underlying biology, and is usually not the case when applying scRNA-seq to characterize a tissue. It is thus beneficial to work with an optimized entry point of the analysis for both the unexperienced user as well as when working with previously unstudied tissue. Looking at the here tested diverse datasets, kallisto potentially provides a better entry point to analyze scRNA-seq data, resulting in increased data quality and clustering quality. Another big advantage is its flexibility concerning the reference input. It only needs a transcriptomic reference as a starting point, which for some organisms might be the only available option or the better annotated version. In addition, kallisto is extremely fast and light weight and can be executed on standard machines [14, 18, 19]. It is under constant maintenance and allows the simple integration of various scRNA-seq platforms, making it extremely versatile [18, 19]. Furthermore, we find it as easy to use as Cell Ranger and can be easily integrated into a custom workflow (see Methods section).

The faster processing time of kallisto also comes with a few disadvantages. One of those is that kallisto does not correct potential sequencing errors in the UMIs, which could lead to incorrect gene detection and expression levels. However, it was recently demonstrated that only little improvement is achieved when UMI sequencing errors are corrected, and therefore it can be considered as a negligible feature [18].

Another potential disadvantage is that reads crossing splice junctions are not filtered out by kallisto. In

contrast, STAR is a splice aware aligner and is thus better suited to deal with such cases. This situation has been addressed in a recent publication and found to be true, but rather rare [18]. Although this could potentially lead to higher, but biased gene detection, for the pineal dataset the additional detected genes were important for the detection of a biologically validated cluster. This suggests that the increased detection rate cannot be attributed entirely to spurious alignment.

Regardless to the number of genes detected, there are strong differences in the UMI counts for some of the detected genes, between kallisto and Cell Ranger (Additional File 1: Fig. S10 & S11 & Additional Files 3 & 5). While for both pipelines, those genes are mainly distributed over all clusters, some with higher UMI counts in the kallisto data can be found in the red cone-like photoreceptor cluster, and most likely led to its identification as a separate cluster. For the particular case of the pineal data, the genes with higher UMI counts in the kallisto data were also cluster markers, but this situation can be different for other datasets.

Another feature that affects the genes detected and the UMI counts is the handling of multi-mapped reads. Currently, both Cell Ranger and kallisto discard reads that map to multiple genes [18]. This feature could increase gene detection rates and quality especially in species with a high degree of paralogous genes [34], like teleost species, due to their shared whole genome duplication event [35]. One of the most popular approaches to correctly count multi-mapped reads is using an expectation maximization (EM) algorithm, which has been integrated into the latest version of STARsolo [36] and alevin [17]. Although we have focused here on the comparison between Cell Ranger and kallisto,

both STARsolo and alevin are also excellent scRNA-seq pre-processing alternatives and produce very similar results [18, 29].

Conclusions
Comparison of the alignment results between Cell Ranger, the standard 10X Genomics-based tool, and the alternative pipeline kallisto, across a wide spectrum of tissues and organisms, revealed higher read alignment and gene detection rates with kallisto across almost all samples. Cell Ranger on the other hand consistently favored higher cell numbers, which mostly included cells with lower median gene counts. Thorough analysis of one of the datasets revealed that clustering analysis is more accurate and biologically meaningful, when kallisto is applied. In order to achieve accurate clustering, it is better to have high quality datasets with high gene detection rates, even if this results in fewer total cells. Depending on the origin of the dataset, we suggest to run alternative pipelines side by side and judge on an individual basis. High gene detection and stringent filtering positively impacts on cell type classification, which is the primary goal for most of the scRNA-seq experiments. Thus, choosing the best possible option is crucial.

Methods
Datasets
A list of all the used datasets and accession numbers can be found in Table 1. The fastq files were directly used for the alignments with no extra trimming of the reads. We stick to the most standard parameters and transcriptomic references (Ensembl genomes & annotations) for Cell Ranger and kallisto to simulate standard usage of these pipelines.

Alignment with Cell Ranger
All datasets were aligned on a cluster node with Cell Ranger version 5.0. The respective genome references and gene transfer format (GTF) files were obtained from Ensembl version 100/101 and prepared with Cell Ranger's mkref function. The alignment was run with standard parameters as described on 10xgenomics.com.

Alignment with kallisto
The index files for the kallisto workflow were generated using either "kb ref" (kb-python 0.24.4; standard parameters (https://github.com/pachterlab/kb_python) to create the index from the same genome and gtf files (Ensembl version 100/101) as for the Cell Ranger references. For creating the index files of just transcriptomic input, "kallisto index --make-unique" was used (https://pachterlab.github.io/kallisto/). The alignment was then performed with "kb count" of the kb-python package. This package conveniently wraps kallisto and bustools into one. For downstream analysis (e.g. Seurat) it is more convenient to work with gene names instead of gene IDs. In order to conveniently change this, we created a helper script to modify the final matrix accordingly. This python script also enables batch processing of several datasets from a sample sheet in an easy to handle command-line interface (CLI). The helper script reads a tsv-file with all the datasets to be aligned, including the respective index files and scRNA-seq library preparation technology. The tool has also the option to create a custom index file, when provided with a fasta-file from BioMart (https://www.ensembl.org/biomart) instead of creating it from a genomic source using "kb ref". See https://github.com/mstemmer/kb-helper for detailed explanation of its usage.

Empty droplet filtering
While Cell Ranger takes care of the empty droplet filtering, the kallisto datasets were imported into R with

busparse 1.3.0, their UMI counts were ranked using DropletUtils 1.9.0 and the empty droplets were removed by defining the inflection point on the resulting knee plot (lower cutoff = 500). The Cell Ranger matrices were loaded from their standard filtered output. We provide the corresponding R scripts with our kb-helper tool (https://github.com/mstemmer/kb-helper).

Downstream processing with seurat

The matrices were converted into objects for seurat v4.0, applying the standard filtering options (min.cells = 3; min.features = 200). Total cell & gene detection, median gene counts & median UMI counts were then extracted from the seurat objects. For better visualization purposes, the cell distribution plots were roughly filtered (nFeature_RNA < 6000 & nCount_RNA < 25,000). The dataset dr-pineal-s2 was chosen for downstream analysis of the data. Therefore, the dataset was further filtered (nFeature_RNA > 200 & nCount_RNA < 15,000 & percent_mito < 30) (Additional file 1: Fig. S8), similar to the original publication [7], with the exception of percent_mito that was not used originally. The data was then log normalized and scaled (using Seurat's default parameters). Variable features were detected (Seurat's default parameters) and used for principal component analysis. PCs 1−20 were used as dimensions of reduction to compute the k.param nearest neighbors (Seurat's FindNeighbors function). Clustering analysis was performed with resolution of 0.9 or 1.2 (Seurat's FindClusters function). UMAP was used to visualize the datasets in 2D, with the same input PCs as the clustering analysis (Seurat RunUMAP function). The top markers for each cluster were computed (Seurat's FindAllMarkers functions) and used for cluster identifications (Fig. 4, Additional file 1: Fig. S9 & Additional file 3). The markers were compared to the original publication [7], while newly detected clusters were identified by comparing their marker genes to what is known in literature. The clustering analysis resulted in sub-clusters of the known pineal clusters (rod-like PhRs, RPE-like and Müller glia-like) as well as the habenula *kiss1* neurons and the leukocytes. The sub-clusters which had similar markers, varying only in expression levels, were merged to simplify the visualization. The sub-clusters before merging, and their respective markers, are illustrated in (Additional file 1: Fig. S9). The R script with all the relevant commands applied in the downstream analysis can be found in Additional File 6 and a full analysis of dr-pineal-s1 can be found in Additional File 2 (see also https://github.com/ishainer/Shainer-and-Stemmer_2021).

Abbreviations

scRNA-seq: Single-cell RNA sequencing; UMI: Unique molecular identifier; MGC: Median gene count; MUC: Median UMI count; gtf: Gene transfer format; zta: Improved zebrafish transcriptome annotation v4.3.2 (Lawson et al., 2020); PhR: photoreceptor; UMAP: Uniform manifold approximation and projection

Supplementary Information

The online version contains supplementary material available at https://doi.org/10.1186/s12864-021-07930-6.

Additional file 1: Fig. S1 Total gene detection of all datasets compared after processing with either kallisto or Cell Ranger. The Venn diagrams show commonly detected number of genes by both pipelines and uniquely detected genes. **Fig. S2** Violin-plots showing distribution of gene and UMI detection per cell of all the analyzed datasets (Table 1) run with the Cell Ranger pipeline. **Fig. S3** Violin-plots showing distribution of gene and UMI detection per cell of all the analyzed datasets (Table 1) run with the kallisto pipeline. **Fig. S4** Cell counts of all datasets compared after processing with either kallisto forced or Cell Ranger. The Venn diagrams show commonly detected cell barcodes by both pipelines and uniquely detected cell barcodes. **Fig. S5** Alignment results of all datasets (Table 1) run with either Cell Ranger or kallisto forced against Ensembl reference. **a** Percent alignment rates of all reads against the reference transcriptome. **b** Total gene detection. **c** Median gene counts over all cells per dataset. **d** Median UMI counts over all cells per dataset. **e** Total cell counts of each dataset. **Fig. S6** Total gene detection of all datasets compared after processing with either kallisto forced or Cell Ranger. The Venn diagrams show commonly detected number of genes by both pipelines and uniquely detected genes. **Fig. S7** Violin-plots showing distribution of gene and UMI detection per cell of all the analyzed datasets (Table 1) run with the kallisto forced pipeline. **Fig. S8** Violin-plots showing distribution of gene and UMI detection per cell of the dr_pineal_s2 dataset after additional filtering for downstream analysis. Run with either Cell Ranger (**a**), kallisto (**b**) or kallisto forced (**c**). **Fig. S9** Downstream analysis of dr_pineal_s2 before cluster merging. **a** 2D visualization using UMAP of Cell Ranger analyzed clusters before merging, with resolution equal to 0.9. Each point represents a single cell, colored according to cell type. The cells were clustered into 21 types. **b** Expression profile of marker genes according to cluster [7] of (**a**). Clusters 0, 1, 8 and 18 are all rod-like PhRs subclusters. They expressed rod-like PhR markers (*exorh*, *gant1*, *gngt1*), but the expression levels differed and resulted in their separation. For simplicity, they were merged and referred as a single rod-like PhRs cluster in the main text. Similarly, cluster 7 and 12 were merged into a single Müller-glia like cluster, clusters 2, 5, 16 were merged into a single RPE-like cluster, clusters 3 and 10 were merged into a single habenula kiss1 cluster and cluster 11 and 19 were merged into a single leukocytes cluster. **c.** 2D visualization using UMAP of Cell Ranger analyzed clusters, with resolution equal to 2. The cells were clustered into 31 types. However, the two different cone-like PhR cell types are still not distinguished from one another. **d** Expression profile of marker genes according to cluster of (**c**). **e** 2D visualization using UMAP of kallisto analyzed dr_pineal_s2 clusters before merging, with resolution equal to 0.9. The cells were clustered into 24 types. **f** Expression profile of marker genes according to cluster of (**c**). Similar to the descried above, clusters 1, 2, 3, 7 and 21 were merged into a single rod-like PhRs cluster, clusters 0, 9, 17 were merged into a single RPE-like cluster, clusters 11 and 12 were merged into a single Müller-glia like cluster, clusters 4, 5 and 20 were merged into a single habenula kiss1 cluster and clusters 13 and 22 were merged into a single leukocytes cluster. **g** 2D visualization using UMAP of kallisto forced analyzed dr_pineal_s2 clusters, with resolution equal to 1.2. The cells were clustered into 27 types. **h** Expression profile of marker genes according to cluster of (**g**). The *col14a1b* gene was only detected in the kallisto and kallisto forced datasets and is the strongest DE marker within the red cone-like cluster (**f, h**). **Fig. S10** Heatmap of genes with higher counts in kallisto pre-processed pineal data. All the UMI counts for both kallisto and Cell Ranger were summed, and the diff_ratio value was calculated ($kallisto_counts − CellRanger_counts kallisto_counts + CellRanger_counts$) for each gene (Additional file 1: Fig. 10). The top 80 diff_ratio genes, as well as the top 20 genes uniquely identified in kallisto were plotted according to the average scaled expression per cluster. **Fig. S11** Heatmap of genes with higher counts in Cell Ranger pre-processed pineal data. All the UMI counts for both kallisto and Cell Ranger were summed, and the diff_ratio

value was calculated

($kallisto_{c}ounts - CellRanger_{c}ounts kallisto_{c}ounts + CellRanger_{c}ounts$) for each gene (Additional file 1: Fig. S11). The top 80 diff_ratio genes, as well as the top 20 genes uniquely identified in Cell Ranger were plotted according to the average scaled expression per cluster.

Additional file 2.

Additional file 3.

Additional file 4.

Additional file 5.

Additional file 6.

Authors' contributions
I.S. wrote and structured the manuscript and analyzed zebrafish pineal dataset. M.S. designed study and analysis pipeline and wrote and structured the manuscript. All authors have read and approved the manuscript.

Availability of data and materials
All data are freely accessible on either the Gene Expression Omnibus (GEO) or the Sequence Read Archive (SRA) on the servers of the National Center for Biotechnology Information (NCBI). The corresponding accession numbers can be found in Table 1. The script for running our kallisto pipeline can be found here: https://github.com/mstemmer/kb-helper. The scripts of the cluster analysis can also be found as R markdown files here: https://github.com/ishainer/Shainer-and-Stemmer_2021.

Declarations

Ethics approval and consent to participate
Not applicable. No animals were used in this study.

Consent for publication
Not applicable.

Competing interests
The authors declare no competing interests.

References
1. Cao C, Lemaire LA, Wang W, Yoon PH, Choi YA, Parsons LR, et al. Comprehensive single-cell transcriptome lineages of a proto-vertebrate. Nature. 2019;571(7765):349–54. https://doi.org/10.1038/s41586-019-1385-y.
2. Davie K, Janssens J, Koldere D, De Waegeneer M, Pech U, Kreft Ł, et al. A single-cell transcriptome atlas of the aging Drosophila brain. Cell. 2018;174: 982–998.e20.
3. Kölsch Y, Hahn J, Sappington A, Stemmer M, António M, Helmbrecht TO, Lele S, Butrus S, Laurell E. Molecular classification of zebrafish retinal ganglion cells links genes to cell types to behavior. 2021;109:645–62.e9. https://linkinghub.elsevier.com/retrieve/pii/S0896627320309624.
4. Packer JS, Zhu Q, Huynh C, Sivaramakrishnan P, Preston E, Dueck H, et al. A lineage-resolved molecular atlas of C. Elegans embryogenesis at single-cell resolution. Science (80-.). 2019;365:eaax1971. https://www.sciencemag.org/lookup/doi/10.1126/science.aax1971.
5. Pandey S, Shekhar K, Regev A, Schier AF. Comprehensive identification and spatial mapping of Habenular neuronal types using single-cell RNA-Seq. Curr Biol. 2018;28:1052–65.e7. https://doi.org/10.1016/j.cub.2018.02.040.
6. Peuß R, Box AC, Chen S, Wang Y, Tsuchiya D, Persons JL, et al. Adaptation to low parasite abundance affects immune investment and

immunopathological responses of cavefish. Nat Ecol Evol. 2020;4(10):1416–30. https://doi.org/10.1038/s41559-020-1234-2.
7. Shainer I, Michel M, Marquart GD, Bhandiwad AA, Zmora N, Ben-Moshe Livne Z, et al. Agouti-related protein 2 is a new player in the teleost stress response system. Curr Biol. 2019;29:2009–2019.e7.
8. Wang W, Hu C-K, Zeng A, Alegre D, Hu D, Gotting K, et al. Changes in regeneration-responsive enhancers shape regenerative capacities in vertebrates. Science (80-.). 2020;369:eaaz3090.
9. Svensson V, Vento-Tormo R, Teichmann SA. Exponential scaling of single-cell RNA-seq in the past decade. Nat Protoc. 2018;13(4):599–604. https://doi.org/10.1038/nprot.2017.149.
10. Zheng GXY, Terry JM, Belgrader P, Ryvkin P, Bent ZW, Wilson R, et al. Massively parallel digital transcriptional profiling of single cells. Nat Commun. 2017;8(1). https://doi.org/10.1038/ncomms14049.
11. Dobin A, Davis CA, Schlesinger F, Drenkow J, Zaleski C, Jha S, et al. STAR: Ultrafast universal RNA-seq aligner. Bioinformatics. 2013;29(1):15–21. https://doi.org/10.1093/bioinformatics/bts635.
12. Kim D, Pertea G, Trapnell C, Pimentel H, Kelley R, Salzberg SL. TopHat2: accurate alignment of transcriptomes in the presence of insertions, deletions and gene fusions. Genome Biol. 2013;14(4):R36. https://doi.org/10.1186/gb-2013-14-4-r36.
13. Wu TD, Nacu S. Fast and SNP-tolerant detection of complex variants and splicing in short reads. Bioinformatics. 2010;26(7):873–81. https://doi.org/10.1093/bioinformatics/btq057.
14. Bray NL, Pimentel H, Melsted P, Pachter L. Near-optimal probabilistic RNA-seq quantification. Nat Biotechnol. 2016;34(5):525–7. https://doi.org/10.1038/nbt.3519.
15. Patro R, Mount SM, Kingsford C. Sailfish enables alignment-free isoform quantification from RNA-seq reads using lightweight algorithms. Nat Biotechnol. 2014;32(5):462–4. https://doi.org/10.1038/nbt.2862.
16. Patro R, Duggal G, Love Ml, Irizarry RA, Kingsford C. Salmon provides fast and bias-aware quantification of transcript expression. Nat Methods. 2017; 14(4):417–9. https://doi.org/10.1038/nmeth.4197.
17. Srivastava A, Malik L, Smith T, Sudbery I, Patro R. Alevin efficiently estimates accurate gene abundances from dscRNA-seq data. Genome Biol. 2019;20(1): 65. https://doi.org/10.1186/s13059-019-1670-y.
18. Melsted P, Booeshaghi AS, Liu L, Gao F, Lu L, Min KH, et al. Modular, efficient and constant-memory single-cell RNA-seq preprocessing. Nat Biotechnol. 2021;39(7):813–8. https://doi.org/10.1038/s41587-021-00870-2.
19. Melsted P, Ntranos V, Pachter L. The barcode, UMI, set format and BUStools. Bioinformatics. 2019;35:4472–3. Available from: https://academic.oup.com/bioinformatics/article/35/21/4472/5487510.
20. Klein AM, Mazutis L, Akartuna I, Tallapragada N, Veres A, Li V, et al. Droplet barcoding for single-cell transcriptomics applied to embryonic stem cells. Cell. 2015;161(5):1187–201. https://doi.org/10.1016/j.cell.2015.04.044.
21. Lun ATL, Riesenfeld S, Andrews T, Dao TP, Gomes T, Marioni JC. EmptyDrops: distinguishing cells from empty droplets in droplet-based single-cell RNA sequencing data. Genome Biol. 2019;20(1):63. https://doi.org/10.1186/s13059-019-1662-y.
22. Macosko EZ, Basu A, Satija R, Nemesh J, Shekhar K, Goldman M, et al. Highly parallel genome-wide expression profiling of individual cells using Nanoliter droplets. Cell. 2015;161(5):1202–14. https://doi.org/10.1016/j.cell.2015.05.002.
23. Griffiths JA, Richard AC, Bach K, Lun ATL, Marioni JC. Detection and removal of barcode swapping in single-cell RNA-seq data. Nat Commun. 2018;9(1): 2667. https://doi.org/10.1038/s41467-018-05083-x.
24. Lawson ND, Li R, Shin M, Grosse A, Yukselen O, Stone OA, et al. An improved zebrafish transcriptome annotation for sensitive and comprehensive detection of cell type-specific genes. Elife. 2020;9:1–76.
25. Lagman D, Callado-Pérez A, Franzén IE, Larhammar D, Abalo XM. Transducin duplicates in the zebrafish retina and pineal complex: differential specialisation after the teleost Tetraploidisation. PLoS One. 2015;10(3): e0121330. https://doi.org/10.1371/journal.pone.0121330.
26. La Manno G, Soldatov R, Zeisel A, Braun E, Hochgerner H, Petukhov V, et al. RNA velocity of single cells. Nature. 2018;560:494–8. http://www.nature.com/articles/s41586-018-0414-6.
27. Du Y, Huang Q, Arisdakessian C, Garmire LX. Evaluation of STAR and Kallisto on single cell RNA-Seq data alignment. G3 Genes|Genomes|Genetics. 2020; 10:1775–83. https://academic.oup.com/g3journal/article/10/5/1775/6026272.
28. Vieth B, Parekh S, Ziegenhain C, Enard W, Hellmann I. A systematic evaluation of single cell RNA-seq analysis pipelines. Nat Commun. 2019; 10(1):4667. https://doi.org/10.1038/s41467-019-12266-7.

29. Schulze Brüning, R., Tombor, L., Schulz, M. H., Dimmeler, S. and John, D. (2021). Comparative Analysis of common alignment tools for single cell RNA sequencing bioRxiv 2021.02.15.430948.

30. Ilicic T, Kim JK, Kolodziejczyk AA, Bagger FO, McCarthy DJ, Marioni JC, et al. Classification of low quality cells from single-cell RNA-seq data. Genome Biol. 2016;17:1–15.

31. Ekström P, Meissl H. The pineal organ of teleost fishes. Rev Fish Biol Fish. 1997;7(2):199–284. https://doi.org/10.1023/A:1018483627058.

32. Falcón, J., Besseau, L. and Boeuf, G. (2006). Molecular and cellular regulation of pineal organ responses. In Fish Physiology, pp 243–306, DOI: https://doi.org/10.1016/S1546-5098(06)25006-4.

33. Cau E, Ronsin B, Bessière L, Blader P. A notch-mediated, temporal asymmetry in BMP pathway activation promotes photoreceptor subtype diversification. PLoS Biol. 2019;17(1):e2006250. https://doi.org/10.1371/journal.pbio.2006250.

34. Deschamps-Francoeur G, Simoneau J, Scott MS. Handling multi-mapped reads in RNA-seq. Comput Struct Biotechnol J. 2020;18:1569–76. https://doi.org/10.1016/j.csbj.2020.06.014.

35. Glasauer SMK, Neuhauss SCF. Whole-genome duplication in teleost fishes and its evolutionary consequences. Mol Gen Genomics. 2014;289(6):1045–60. https://doi.org/10.1007/s00438-014-0889-2.

36. Kaminow B, Yunusov D, Dobin A, Spring C. (2021). STARsolo : accurate, fast and versatile mapping / quantification of single-cell and single-nucleus RNA-seq data. bioRxiv. 2021.05.05.442755. https://doi.org/10.1101/2021.05.05.442755.

Publisher's Note

Springer Nature remains neutral with regard to jurisdictional claims in published maps and institutional affiliations.